Journal of Power Sources 297 (2015) 202–207

Contents lists available at ScienceDirect

Journal of Power Sources

journal homepage: www.elsevier.com/locate/jpowsour

Template-directed fabrication of porous gas diffusion layer for magnesium air batteries

Yejian Xue, He Miao**, Shanshan Sun, Qin Wang, Shihua Li, Zhaoping Liu*

Ningbo Institute of Materials Technology and Engineering, Chinese Academy of Sciences, No. 519, Zhuangshi Road, Zhenhai District, Zhejiang 315201, PR China

HIGHLIGHTS

- Preparation of the interconnected regular pores in the GDL.
- Gas permeability of the GDL with the regular pores was improved.
- P_{max} of the Mg air batteries with the regular porous GDL was elevated.
- The porous GDL exhibited the improved the long term stability.

ARTICLE INFO

Article history:
Received 6 May 2015
Received in revised form
16 June 2015
Accepted 25 June 2015
Available online xxx

Keywords:
Porous gas diffusion layer
Mg air battery
Fuel cell
Silica template
Carbon fiber felt

ABSTRACT

The uniform micropore distribution in the gas diffusion layers (GDLs) of the air-breathing cathode is very important for the metal air batteries. In this work, the super-hydrophobic GDL with the interconnected regular pores is prepared by a facile silica template method, and then the electrochemical properties of the Mg air batteries containing these GDLs are investigated. The results indicate that the interconnected and uniform pore structure, the available water-breakout pressure and the high gas permeability coefficient of the GDL can be obtained by the application of 30% silica template. The maximum power density of the Mg air battery containing the GDL with 30% regular pores reaches 88.9 mW cm^{-2} which is about 1.2 times that containing the pristine GDL. Furthermore, the GDL with 30% regular pores exhibits the improved the long term hydrophobic stability.

1. Introduction

Recently, there has been a strong global incentive to develop electric vehicles (EVs) to reduce petroleum oil dependence and mitigate greenhouse gas emission [1,2]. But there is a great obstacle to develop the EVs because of the high cost and insufficient energy density of the state-of-art lithium ion batteries. In the past few years, metal air batteries have received revived interest due to their high energy density, low cost and friendly environment [3,4].

Metal air batteries feature with the electrochemical coupling of a metal negative electrode to an air-breathing positive electrode through an aqueous solution electrolyte [5]. The cathode structure of the metal air batteries which includes the current collecting layer, the gas diffusion layer and catalyst layer are similar with that of the low temperature fuel cells [6,7]. Among them, the gas diffusion layer (GDL) admits continuous and inexhaustible oxygen from the surrounding air to reach the three-phase boundary (TBP) between air, liquid electrolyte and solid electrode catalyst to occur the oxygen reduction reaction. Thus, an ideal GDL is expected to possess the properties with the waterproof structure to avoid the water flooding, high electronic conductivity to transfer the electron, and high oxygen permeation rate to reduce the concentration polarization.

The electrochemical reactions of the Mg-air batteries can be described by the Equations (1)–(3) [13]. As can be seen in the equations, the theoretical open cell voltage of the Mg-air batteries was 3.09 V, but the as-measured values are usually smaller than 2 V due to the large polarization caused by the sluggish cathode reaction and the self-corrosion of Mg anode [28].

* Corresponding author.
** Corresponding author.
E-mail addresses: miaohe@nimte.ac.cn (H. Miao), liuzp@nimte.ac.cn (Z. Liu).

http://dx.doi.org/10.1016/j.jpowsour.2015.06.141
0378-7753/

Anode reaction: $Mg + 2OH^- \rightarrow Mg(OH)_2 + 2e^- - 2.69\ V$ (1)

Cathode reaction: $1/2O_2 + H_2O + 2e^- \rightarrow 2OH^- + 0.4\ V$ (2)

Overall reaction: $Mg + 1/2O_2 + H_2O \rightarrow Mg(OH)_2 + 3.09\ V$ (3)

It was reported that the energy consumption for each kilogram of Mg produced by the traditional Pidgeon process was 280 MJ [29,30]. Whereas, the theoretical and as-measured electrochemical energy of the Mg with the same weight were 24.5 MJ and 1.8 MJ with the assumption of the theoretical and as-measured power density of Mg-air batteries was 6800 Wh kg^{-1} and 500 Wh kg^{-1}, respectively. The energy loss from the Mg production to the Mg air batteries is serious. Therefore, decreasing the energy consumption of Mg production and improving the electrochemical properties of the Mg-air batteries are two important factors to enhance the energy utilization of the Mg anode. In general, the performances of the Mg-air batteries can be related to many factors, such as the compositions of the Mg-based anode, the ORR catalysts, the electrolyte additives, and the GDLs.

A traditional GDL is usually composed of carbon materials (such as carbon powder [8,9], carbon nano-fibers (CNF) [10], carbon nanotubes (CNT) [11,12] and carbon fiber felt (CFF) [13]) as the electronic conduction support and the polytetrafluoroethylene (PTFE) binder as the water proof material to avoid flooding the pores by the electrolyte. Among them, the GDL made by CFF/PTFE has been extensively used in the metal air batteries. The pores in the GDL with the proper quantity and dimension are very important for the properties of the metal air batteries. It will be very hard for the gas diffusion, and subsequently increase the concentration polarization of the metal air batteries containing the GDL with a few or small pores. Whereas, the electrolyte will be flooded the GDL and block the transport of oxygen to the TBP as the GDL contains too many or large pores. In addition, the gas diffusion coefficient of the GDL always decreases during long-term operation because the pore channels are readily to be clogged by the particles in air. It is well known that the uniform micropore regulation and distribution in the GDL can effectively alleviate its geometry variation, and then keep the diffusion coefficient of oxygen unchanged after long term operation [14,15].

Unfortunately, it is difficult to make the uniform porous PTFE by a typical polymer melt foaming process because its high molecular weight and melt viscosity [16]. Even if the template method is popular for the porous material fabrication, the templates are very hard to remove from the PTFE bulk due to its low melting point (327 °C) and superbly hydrophobic property. Up to now, the porous PTFE have still been prepared by the traditional method of extrusion, rolling, and stretching.

In this work, a facile method with the silica as the hard template to create the regular and uniform pores in the PTFE/CFF GDL was applied, and then the electrochemical properties of the magnesium air batteries containing this GDL were investigated. To the best of our knowledge, it is almost the first report about the porous PTFE fabricated by the traditional template method. This template method to create the regular and uniform pores in the PTFE can also be used in the other areas, such as the fabrication of the porous PTFE air cathode for microbial fuel cells, the porous PTFE substrate for redox flow battery, the PTFE membrane with highly ordered pores distribution for the desalination, the gas diffusion layer (GDL) of proton exchange membrane (PEM) with the desired monodisperse pores for water management and the hierarchical porous materials for the sieving membrane or the catalyst support [17–25], besides the fabrication of the GDL for the metal air batteries in this work.

2. Experimental

2.1. Fabrication of GDL and cathode

A facile fabrication approach of the PTFE/CFF GDL with regular pores was illustrated in Fig. 1. The 60 wt.% PTFE suspension (Shanghai 3F New Material Co. Ltd. of China) was diluted from 10 to 40 wt.% by the deionized water. The commercial silica spheres (Sinopharm Chemical Reagent Co. Ltd. of China) with a relatively uniform particle size of 2 μm were added into the diluted PTFE solution and dispersed uniformly. The carbon fiber felts (CFFs) (Haoshi Carbon Fiber Material Co. Ltd. of China) were immersed into the mixture of the diluted PTFE suspension and the silica spheres, and then dried at the temperature of 50 and 80 °C for 8 and 24 h, respectively. Then, the immersed CFFs were sintered at 350 °C for 1 h. After sintering, the prepared GDLs were pressed for 2 min under a pressure of 10 MPa at the temperature of 200 °C, and then etched by the mixture solution of 50 wt.% ethanol, 20 wt.% HF and 30 wt.% H_2O to remove the silica templates. In this work, the GDL samples before and after the pore creation are denoted as PTFE-x and PTFE-x/CFF-y, where x and y represent the concentration of the PTFE suspension and the percent of SiO_2 in the mixture of PTFE and SiO_2, respectively.

The cathodes with the as-prepared GDLs were made by the following procedure. The homemade MnO_2/C catalyst was uniformly dispersed in the mixture of the PTFE suspension and the terpineol solvent to prepare the catalyst slurry. The catalyst slurry was coated on the surface of the GDLs with the loading of 3 mg cm^{-2} by the screen-printing method. The cathodes were dried at 80 °C for 2 h, and then sintered at 350 °C for 1 h. The as-prepared cathode was finally pressed with Ni foam as current collector for 1 min under a pressure of 2 MPa at the temperature of 200 °C.

2.2. Characterizations and test

The morphologies of the GDLs and SiO_2 powders were examined by the scanning electron microscope (SEM, FEI Quanta FEG 250). The contact angles of the electrolyte and ethanol on the GDLs were determined by the contact angle measurement system (Dataphysics, OCA20, Germany) at 25 °C. The bulk porosity of the samples was tested by an analog Archimedes measurement in the decane solution which could flood both the hydrophilic and hydrophobic pores [26]. The hydrophilic porosity of the GDLs was measured by a homemade apparatus. The sample was placed horizontally in the quartz tube at room temperature. Water vapour carried by the air flowed through the sample. In this process, the capillary condensation occurred in the hydrophilic pores and the liquid water accumulated with time till it filled the hydrophilic pores. By weighing the sample before and after the measurement, the hydrophilic porosity could be calculated. Hydrophobic porosity was obtained by subtracting the hydrophilic porosity from the bulk porosity. For testing the electrochemical properties of the Mg air batteries containing the GDLs mentioned above, the 10 wt. % sodium chloride solution, as-prepared cathode and magnesium alloy of AZ61 were used as the electrolyte, cathode and anode, respectively. And then the Mg air battery was tested in the homemade testing house at the room temperature. The active area of the cathode of the Mg air battery was $2 \times 2\ cm^2$. And the I–V and I–P curves of the Mg air batteries containing the different GDLs were obtained by the cell testing system (LAND CT2001A, China). The morphologies and elemental compositions of the aged cathodes were detected by scanning electron microscope (SEM, FEI Quanta FEG 250) with Energy-dispersive X-ray Spectroscopy (EDS).

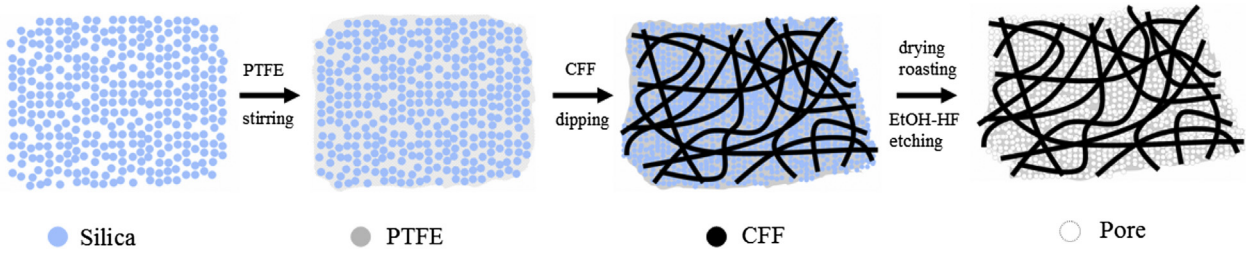

Fig. 1. Schematic illustration of the fabrication procedure of the regular porous PTFE/CFF GDLs.

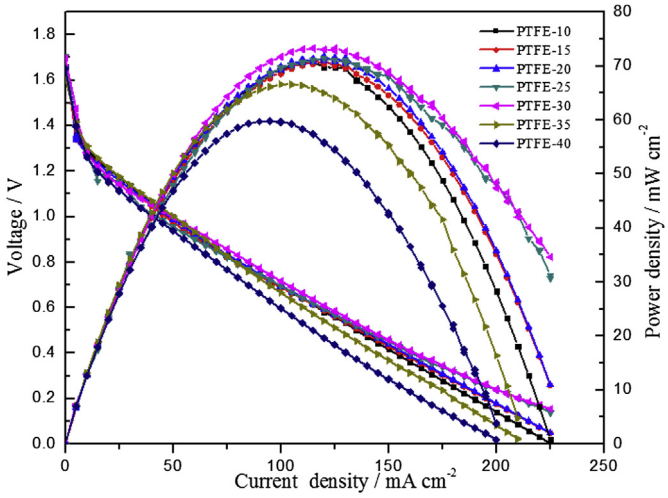

Fig. 2. I–V and I–P curves of the Mg air batteries containing the PTFE-x (x = 10–40) GDLs.

3. Results and discussion

The current density-voltage (I–V) and current density-power density (I–P) curves of the Mg air batteries with the PTFE-x GDLs are showed in Fig. 2. As can be seen from Fig. 2, the maximum power density (P_{max}) of the battery with the PTFE-30 GDL reaches 73.3 mW cm^{-2}, which is the highest value for all the GDLs. So the PTFE-30 GDL is selected for the further investigation. On the purpose of removing the silica template, the contact angles of the etching solution with different alcohol content on the PTFE-30/CFF-30 GDL with the silica template are measured and shown in Fig. 3. For accelerating the etching process, the etching solution containing 50 wt.% ethanol with the contact angle of 79.3° on the PTFE-30/CFF-30 GDL was selected.

Fig. 4 shows the SEM images of the PTFE-30/CFF-y GDLs. It can be seen clearly that a regular porous structure is formed for all the GDLs after pore creation, while almost no regular pore can be found in the GDLs without pore creation. Further, the interconnected structures of the regular pores in GDLs are formed when y is more than 30 (Fig. 4d and e). But the porous structure collapses as y value is more than 50 (Fig. 4f). Table 1 lists the PTFE content, bulk porosity, hydrophilic porosity and hydrophobic porosity of the different GDLs. It can be noted from Table 1 that the PTFE content in the PTFE-30/CFF-y GDLs decreases from 62.6 to 48 wt.% with the increase of y from 0 to 50. Correspondingly, the hydrophobic porosity [26] increases from 34.5 to 43.4%. In addition, the PTFE content, bulk porosity, hydrophilic porosity, and hydrophobic porosity of the PTFE-30/CFF-30 GDL are 52.7%, 40%, 0.8% and 39.2%, respectively, which are almost similar to those of the PTFE-25 GDL. Fig. 5 shows the water-breakout pressure [23,24] and gas permeability coefficient [27] of PTFE-30/CFF-y GDLs. The water-breakout pressure of the GDLs decreases from 9898 to 6468 Pa, while the gas permeability coefficient increases from 2.21 × 10^{-14} m^2 to 4.91 × 10^{-14} m^2 with the increase of y from 0 to 50.

Fig. 6 Shows the I–V and I–P curves of the Mg air batteries containing the different GDLs. From Fig. 5, the maximum power density (P_{max}) of the batteries increases from 73.3 (y = 0) to 89.9 mW cm^{-2} (y = 40), and then decreases abruptly to 67.5 mW cm^{-2} (y = 50) with the increase of y from 0 to 50. And the P_{max} of the battery with the PTFE-30/CFF-30 GDL is about 21.3% higher than that of the batteries containing PTFE-30/CFF-0 GDL, which indicates that the proper regular pores in the GDLs are favor to P_{max} of the Mg air batteries. Considering that the water-breakout pressure of the PTFE-30/CFF-30 GDL is much higher than that of the PTFE-30/CFF-40 GDL, the PTFE-30/CFF-30 GDL is selected for the further study.

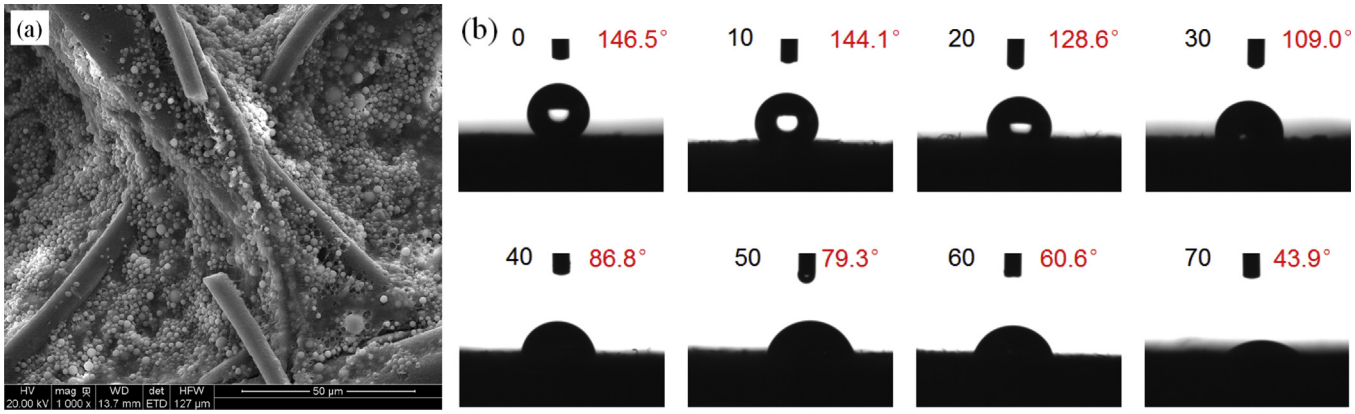

Fig. 3. SEM image of the PTFE-30/CFF-30 GDL before removing the silica template (a) and the contact angles of the etching solution with the different alcohol content on the PTFE-30/CFF-30 GDL (b).

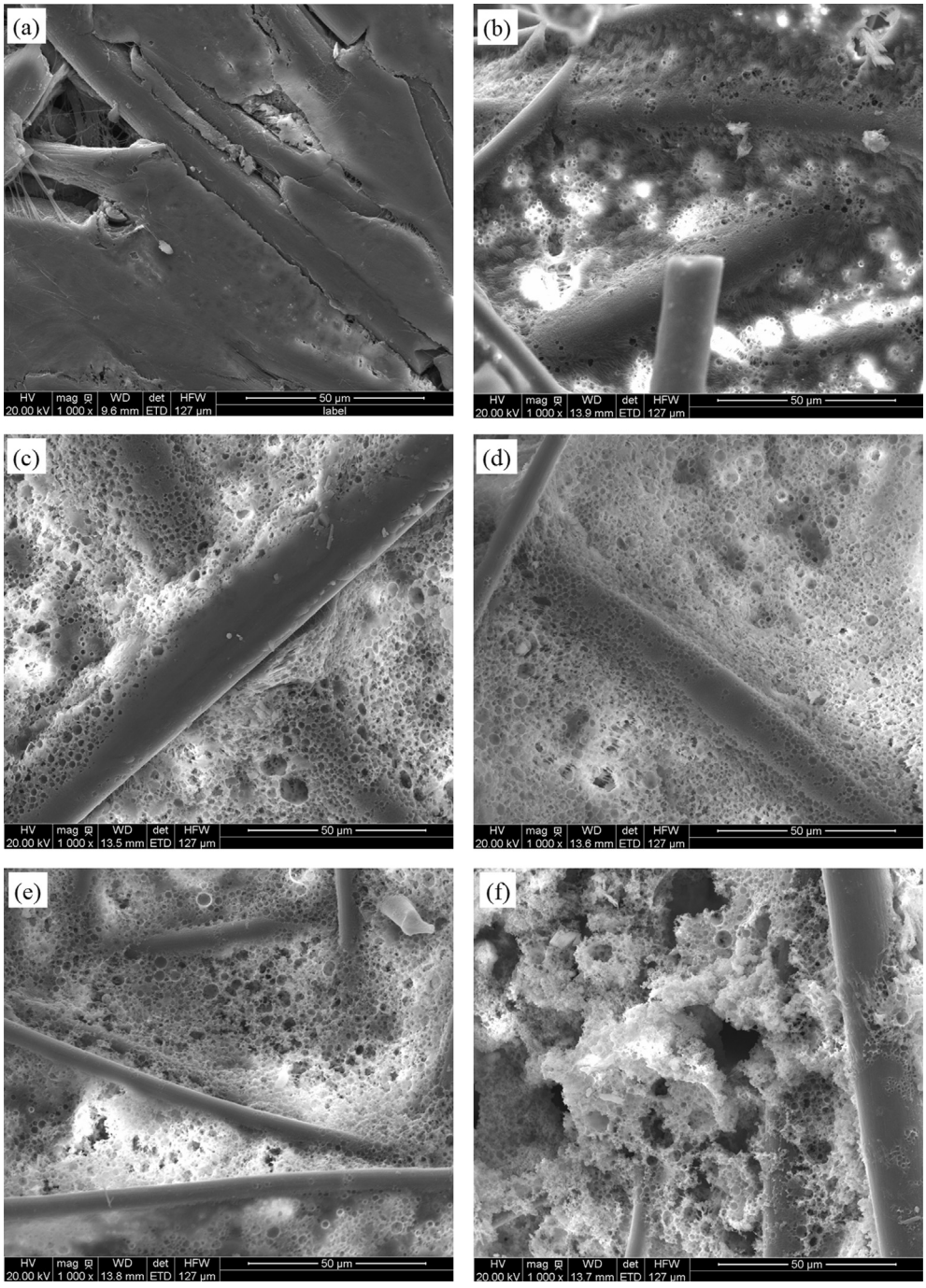

Fig. 4. SEM images of the PTFE-30/CFF-y GDLs: y = 0 (a); y = 10 (b); y = 20 (c); y = 30 (d); y = 40 (e); y = 50 (f).

Fig. 7 shows the I–V and I–P curves of the batteries with the PTFE-30/CFF-30 and PTFE-30/CFF-0 GDLs before and after the discharging operation under the constant current density of 50 mA cm^{-2} for 8 h, respectively. After the discharging operation, the electrolyte and anode are replaced with the fresh ones, and then the I–V and I–P curves are measured. As can be seen from the figure, the P_{max} of the batteries with the PTFE-30/CFF-30 and PTFE-30/CFF-0 GDLs decreases to 85.8 mW cm^{-2} and 60.9 mW cm^{-2}, corresponding to 96.5% and 83.1% of that before the discharging operation, respectively. The degradation of the batteries can be mainly attributed to the blocking of the GDL pores by $Mg(OH)_2$ because the fresh anode and electrolyte are replaced. This means that the proper regular pores in the GDLs are inert to be blocked.

In order to investigate the degradation mechanism of the Mg air batteries containing the PTFE-30/CFF-30 and PTFE-30/CFF-0 GDLs, the hydrophobic properties of the two GDLs were evaluated by testing the contact angle of the 10 wt.% sodium chloride solution on them. As can be seen from Fig. 8a, the contact angles of the NaCl solution on the fresh PTFE-30/CFF-0 and PTFE-30/CFF-30 GDLs are 136.0° and 135.6°, respectively. While the contact angles of the NaCl solution on the aged PTFE-30/CFF-0 and PTFE-30/CFF-30 GDLs decrease to 68° and 127.2°, respectively. This suggests that the

Table 1
PTFE concentration, percent of SiO_2 in the mixture of PTFE and SiO_2, PTFE content of the GDL, bulk porosity, hydrophilic porosity and hydrophobic porosity of the PTFE-x and PTFE-30/CFF-y GDLs.

Sample	PTFE suspension concentration (wt.%)	SiO_2/PTFE content in suspension (wt.%)	PTFE content in GDL (wt.%)	Bulk porosity (%)	Hydrophilic porosity (%)	Hydrophobic porosity (%)
PTFE-10	10	0	36.5	50.1	2.8	47.3
PTFE-15	15	0	43.3	45.7	1.2	44.5
PTFE-20	20	0	48.2	41.5	0.8	40.7
PTFE-25	25	0	51.8	40.6	0.5	40.1
PTFE-30 (/CFF-0)	30	0	62.6	34.7	0.2	34.5
PTFE-35	35	0	73.9	30.3	0.1	30.2
PTFE-40	40	0	76.4	26.2	0.1	26.1
PTFE-30/CFF-10	30	10	58.9	35.4	0.4	35.0
PTFE-30/CFF-20	30	20	55.6	39.5	0.7	38.8
PTFE-30/CFF-30	30	30	52.7	40.0	0.8	39.2
PTFE-30/CFF-40	30	40	50.2	42.6	0.9	41.7
PTFE-30/CFF-50	30	50	48.0	45.0	1.6	43.4

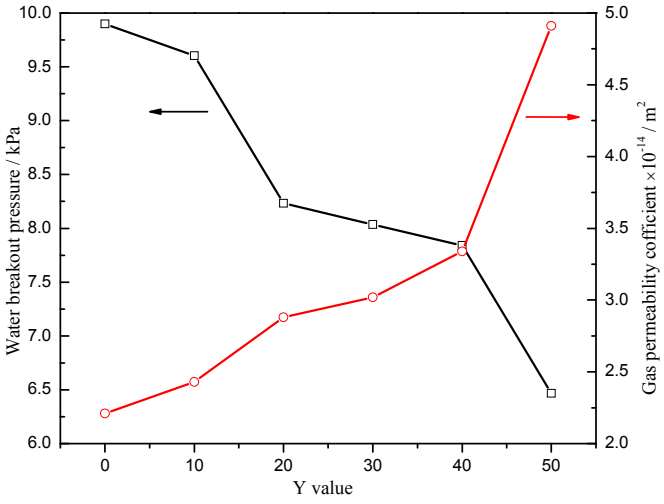

Fig. 5. Water-breakout pressure and gas permeability coefficient of the PTFE-30/CFF-y (y = 0–50) GDLs.

proper regular pores in the GDLs can greatly improve the hydrophobic stability during the discharge operation. Moreover, Fig. 8b and c show the elemental distribution of Na, Cl and Mg on the surface of the aged PTFE-30/CFF-30 and PTFE-30/CFF-0 GDLs. It can be found that the content of Mg, Na and Cl on the PTFE-30/CFF-0 GDL is much more than that of the PTFE-30/CFF-30 GDL. This implies that the proper regular pores in the GDL can effectively suppress the infiltration of the electrolyte and $Mg(OH)_2$ because of its long term hydrophobic stability.

4. Conclusions

In summary, the interconnected regular pores can be successfully fabricated in the PTFE/CFF GDL by a facile template method. Compared with the pristine GDL, the P_{max} of the Mg air battery increases from 73.3 to 88.9 mW cm^{-2} with the increase of 30% regular pores in the GDL. Also, the long term hydrophobic stability of the GDL can be obviously improved by the introduction of the regular pores. Furthermore, the strategy of the pore creation presented in this work can be expended as a general method to fabricate porous PTFE component.

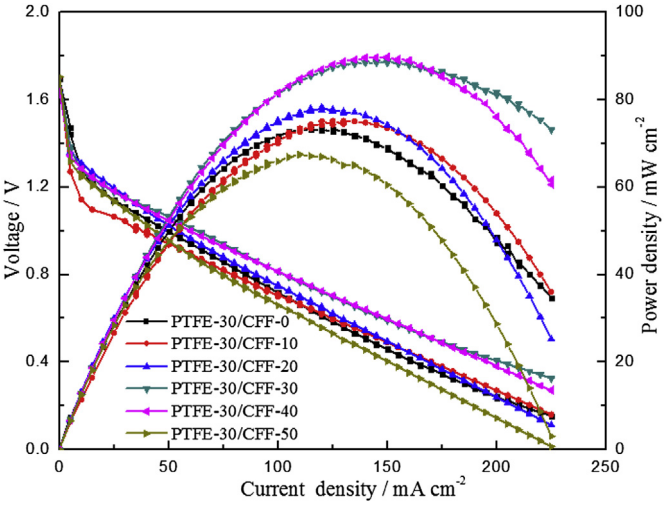

Fig. 6. I–V and I–P curves of the Mg air batteries containing the PTFE-30/CFF-y (y = 0–50) GDLs.

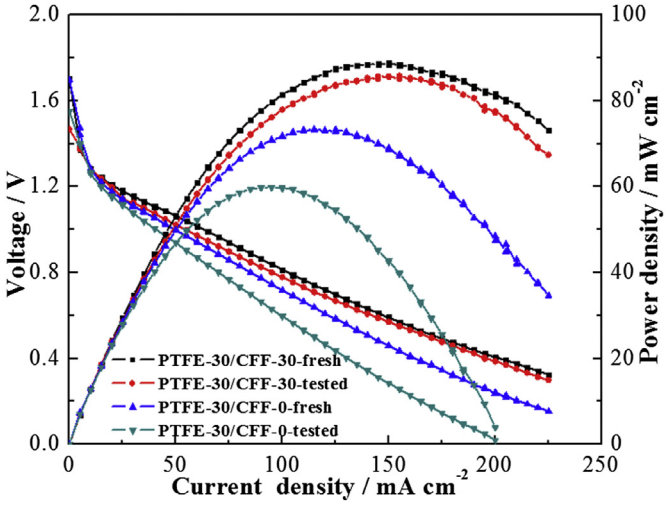

Fig. 7. I–V and I–P curves of the Mg air batteries containing the PTFE-30/CFF-0 and PTFE-30/CFF-30 GDLs before and after the discharge operation for 8 h at the current density of 50 mA cm^{-2}.

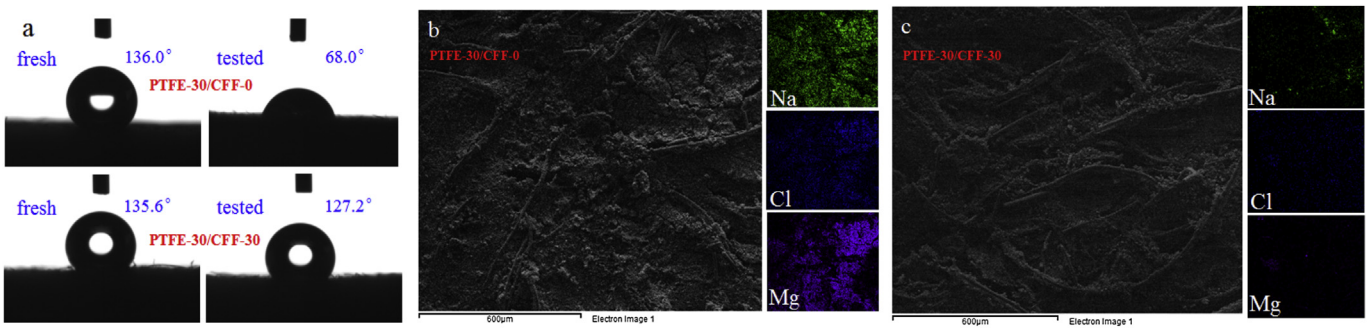

Fig. 8. Contact angle of the 10 wt.% NaCl on the PTFE-30/CFF-0 and PTFE-30/CFF-30 GDLs before and after the discharge operation for 8 h (a); elemental distribution of the PTFE-30/CFF-0 (b) and PTFE-30/CFF-30 GDLs after the discharge operation for 8 h (c).

Acknowledgements

The authors are grateful for the financial supports from the Ningbo Natural Science Foundation (No. 2015A610251), National Natural Science Foundation of China (Grant No. 21103212) and Ningbo Science and Technology Innovation Team (2012B82001).

References

[1] J.H. Williams, A. DeBenedictis, R. Ghanadan, A. Mahone, J. Moore, W.R. Morrow III, S. Price, M.S. Torn, Science 335 (2012) 53–59.
[2] M. Armand, J.M. Tarascon, Nature 451 (2008) 652–657.
[3] Y.G. Li, H.J. Dai, Chem. Soc. Rev. 43 (2014) 5257–5275.
[4] S. Jin, A.G. Hubert, Y. Naoaki, N. Haruyuki, B.G. John, S.H. Yang, Nat. Chem. 3 (2011) 546–550.
[5] Z.L. Wang, D. Xu, J.J. Xu, X.B. Zhang, Chem. Soc. Rev. 43 (2014) 7746–7786.
[6] F.Y. Cheng, J. Chen, Chem. Soc. Rev. 41 (2012) 2172–2192.
[7] J.S. Lee, S.T. Kim, R.G. Cao, N.S. Choi, M.L. Liu, K.T. Lee, J. Cho, Adv. Energy Mater. 1 (2011) 34–50.
[8] J. Liu, L.H. Jiang, Q.W. Tang, E.D. Wang, L.T. Qi, S.L. Wang, G.Q. Sun, Appl. Catal. B Environ. 148–149 (2014) 212–220.
[9] C.C. Yang, Int. J. Hydrogen Energy 29 (2004) 135–143.
[10] W.Q. Yang, S.H. Yang, J.S. Guo, G.Q. Sun, Q. Xin, Carbon 45 (2007) 397–401.
[11] G.Q. Zhang, X.G. Zhang, Y.G. Wang, Carbon 42 (2007) 3097–3102.
[12] H. Huang, W.K. Zhang, M.C. Li, Y.P. Gan, J.H. Chen, Y.F. Kuang, J. Colloid Interface Sci. 284 (2005) 593–599.
[13] C.Z. Shu, E.D. Wang, L.H. Jiang, G.Q. Sun, Int. J. Hydrogen Energy 38 (2013) 5885–5893.
[14] Z. Ma, P.C. Pei, K.L. Wang, X.Z. Wang, H.C. Xu, Y.F. Liu, G.L. Peng, J. Power Sources 274 (2015) 56–64.
[15] P.C. Pei, K.L. Wang, Z. Ma, Appl. Energy 128 (2014) 315–324.
[16] T. Kurose, T. Akahashi, K. Koyama, J. Porous Mater. 11 (2004) 173–181.
[17] Q. Deng, X.Y. Li, J. Zuo, A. Ling, B.E. Logan, J. Power Sources 195 (2010) 1130–1135.
[18] G.R. Molaeimanesh, M.H. Akbari, J. Power Sources 258 (2014) 89–97.
[19] S. Kim, B.H. Jeong, B.K. Hong, T.S. Kim, J. Power Sources 270 (2014) 342–348.
[20] N. Khajeh-Hosseini-Dalasm, T. Sasabe, T. Tokumasu, U. Pasaogullari, J. Power Sources 266 (2014) 213–221.
[21] Y.P. Sheng, S.L. Song, X.L. Wang, L.Z. Song, C.J. Wang, H.H. Sun, X.Q. Niu, Electrochim. Acta 56 (2011) 8651–8656.
[22] C.M. Hwang, M. Ishida, H. Ito, T. Maeda, A. Nakano, Y. Hasegawa, N. Yokoi, A. Kato, T. Yoshida, Int. J. Hydrogen Energy 36 (2011) 1740–1753.
[23] W.H. He, J. Liu, D. Li, H.M. Wang, Y.P. Qu, X. Wang, Y.J. Feng, J. Power Sources 267 (2014) 219–226.
[24] M. Mortazavi, K. Tajiri, Int. J. Hydrogen Energy 39 (2014) 9409–9419.
[25] C. Ponce de León, A. Frías-Ferrer, J. González-García, D.A. Szánto, F.C. Walsh, J. Power Sources 160 (2006) 716–732.
[26] X.L. Wang, H.M. Zhang, J.L. Zhang, H.F. Xu, Z.Q. Tian, J. Chen, H.X. Zhong, Y.M. Liang, B.L. Yi, Electrochim. Acta 51 (2006) 4909–4915.
[27] M.V. Williams, E. Begg, L. Bonville, H.R. Kunz, J.M. Fenton, J. Electrochem. Soc. 151 (8) (2004) A1173–A1180.
[28] W.Y. Li, C.S. Li, C.Y. Zhou, H. Ma, J. Chen, Angew. Chem. Int. Ed. 45 (2006) 6009–6012.
[29] S. Ramakrishnan, P. Koltun, Resour. Conserv. Recycl. 42 (2004) 49–64.
[30] J.D. Du, W.J. Han, Y.H. Peng, J. Clean. Prod. 18 (2010) 112–119.